19th Brazilian Congress of Thermal Sciences and Engineering
November 6th–10th, 2022, Bento Gonçalves - RS - Brazil

ENC-2022-0088
ACCURACY ANALYSIS OF GRADIENT RECONSTRUCTION TECHNIQUES FOR THE DISCRETE SOLUTION OF THE GAS DYNAMICS EQUATIONS

Frederico Bolsoni Oliveira
Instituto Tecnológico de Aeronáutica – DCTA/ITA, 12228-900, São José dos Campos, SP, Brazil.
fredericobolsoni@gmail.com

João Luiz F. Azevedo
Instituto de Aeronáutica e Espaço – DCTA/IAE/ACE-L, 12228-904, São José dos Campos, SP, Brazil.
joaoluiz.azevedo@gmail.com

Abstract. *Three different gradient reconstruction techniques are analyzed in the context of a cell-centered, finite volume formulation for the discrete solution of the gas dynamics equations. Attention is given to the usage of quadrilateral meshes. The quality of the results is assessed by considering two different test cases. The first one is the two-dimensional, zero pressure gradient, flat plate. It is used to identify possible differences between each scheme when facing a geometrically simple problem. The second one is the transonic OAT15A airfoil, used to display the general behavior of each scheme when a shock wave is present in the solution domain. All cases are simulated using a code developed in-house, in which Roe's second-order, TVD, numerical flux is employed in the discretization of the inviscid flux vectors. Viscous flux vectors are discretized by applying a standard centered scheme. Turbulence effects are taken into account by making use of the negative Spalart-Allmaras turbulence model. Further comparisons are made with experimental and numerical data available in the literature. No meaningful difference is observed between each discretization scheme, at least for the cases considered here, and excellent agreement is obtained between the computed solutions and the expected results.*

Keywords: *Finite Volume, Gradient Reconstruction, Negative Spalart-Allmaras Model, Flat Plate, OAT15A Airfoil*

1. INTRODUCTION

Numerical solutions of physical models are often sought in engineering applications due to their ability to provide insights to the users regarding the complex physics of a given problem. Depending on the application, these results can help engineers design better and more efficient products at lower costs. Therefore, any improvements to well established numerical procedures are welcomed by the general community. In the realm of computational fluid dynamics (CFD), finite volume (FV) formulations have been successfully used throughout the past few decades to numerically solve, among others, different levels of approximation of the gas dynamics equations (Hirsch, 1988b). An important step of cell-centered FV formulations is the evaluation of discrete properties at cell interfaces, including their gradients. These values, however, are usually not readily available and, therefore, a reconstruction scheme must be employed.

It has been previously reported in the literature that the use of different gradient reconstruction techniques can drastically change the outcome of viscous fluid simulations (Jalali *et al.*, 2014). The effects vary from changing the overall robustness of the CFD algorithm being employed, to modifying or dissipating fluid structures that are present in the solution field. Unfortunately, no single gradient reconstruction procedure has been found so far to be suited for all applications. The present study is inserted in this context, and aims to provide numerical data for better understanding the effects that different gradient reconstruction techniques have over the numerical solution of compressible turbulent flows when used with quadrilateral meshes. It is hoped that the study here presented contributes such that CFD users can make better judgment regarding which gradient reconstruction technique to use when facing problems with similar configurations.

In the current work, the three-dimensional gas dynamics are modeled using the compressible Reynolds-averaged Navier-Stokes (RANS) equations. In the literature, they are also termed the Favre-averaged Navier-Stokes equations (Hirsch, 1988b), coupled with conservation laws for mass and energy. These equations are discretized in a cell-centered FV framework by using Roe's flux-difference splitting scheme for the reconstruction of the convective fluxes (Roe, 1981; Bigarella and Azevedo, 2009, 2012). A second-order, total-variation diminishing (TVD) version of the scheme is imple-

mented by using a piecewise linear reconstruction of the solution (Barth and Jespersen, 1989), coupled with Venkatakrishnan's limiter (Venkatakrishnan, 1995). The closure problem, inherent to the RANS equations, is solved by making use of the negative Spallart-Allmaras (SA-neg) turbulence model (Spalart and Allmaras, 1992; Allmaras *et al.*, 2012; Rumsey, 2022). Average cell gradients are computed by using a volume-weighted Green-Gauss formulation. Furthermore, property gradients at cell interfaces are computed using three different reconstruction schemes: $A00$, $A0E$ and $AJ0$, whose naming conventions follow Jalali *et al.* (2014). More details about each formulation will be provided in the forthcoming sections.

Two test cases are considered here. The first one is the two-dimensional, zero pressure gradient, turbulent flat plate (Rumsey, 2022). It is mainly used to identify possible differences between the gradient reconstruction schemes when facing a geometrically simple problem. The second one is the transonic OAT15A airfoil (Roddle and Archambaud, 1994; Bigarella and Azevedo, 2009, 2012). This test case intends to illustrate the performance of each procedure when a shock wave is present in the domain. All cases are simulated using a code developed in-house, BRU3D (Bigarella and Azevedo, 2009, 2012). This introduction section is followed by a presentation of the numerical formulation employed in the present work. Then, a brief description of the test cases is made, accompanied by the obtained results and the concluding remarks.

2. NUMERICAL FORMULATION

2.1 General Method for Solving the Gas Dynamics Equations

The RANS equations are used to model the gas dynamics in the present effort. They can be written as

$$\frac{\partial \vec{Q}}{\partial t} + \vec{\nabla} \cdot \vec{\mathcal{F}}(\vec{Q}, \overrightarrow{\nabla Q}) \equiv \frac{\partial \vec{Q}}{\partial t} + \vec{\nabla} \cdot \left[\vec{\mathcal{F}}_e(\vec{Q}) - \vec{\mathcal{F}}_v(\vec{Q}, \overrightarrow{\nabla Q}) \right] = 0 \,, \tag{1}$$

where $\vec{Q}$ is the vector of conserved variables. Furthermore, $\vec{\mathcal{F}}$ is a vector of geometric vectors, such that

$$\vec{\mathcal{F}}_e(\vec{Q}) \equiv \vec{E}_e(\vec{Q})\,\hat{\imath} + \vec{F}_e(\vec{Q})\,\hat{\jmath} + \vec{G}_e(\vec{Q})\,\hat{k} \,, \tag{2}$$

and

$$\vec{\mathcal{F}}_v(\vec{Q}, \overrightarrow{\nabla Q}) \equiv \vec{E}_v(\vec{Q}, \overrightarrow{\nabla Q})\,\hat{\imath} + \vec{F}_v(\vec{Q}, \overrightarrow{\nabla Q})\,\hat{\jmath} + \vec{G}_v(\vec{Q}, \overrightarrow{\nabla Q})\,\hat{k} \,, \tag{3}$$

with

$$\vec{\mathcal{F}} \equiv \vec{\mathcal{F}}_e - \vec{\mathcal{F}}_v \,. \tag{4}$$

Vectors $\vec{E} \equiv \vec{E}_e - \vec{E}_v$, $\vec{F} \equiv \vec{F}_e - \vec{F}_v$ and $\vec{G} \equiv \vec{G}_e - \vec{G}_v$ are the flux vectors associated with the Cartesian coordinate triad x, y and z, respectively. In the same manner, $\hat{\imath}$, $\hat{\jmath}$ and $\hat{k}$ are unit vectors aligned with the same triad, respectively. The subscripts e and v refer to the inviscid and viscous components of each flux vector. The functional relation that exists between each vector and $\vec{Q}$ and $\overrightarrow{\nabla Q}$ has been explicitly written. This has been done in order to emphasize that only the viscous part of this formulation requires the evaluation of $\overrightarrow{\nabla Q}$. The complete description of each flux vector is well known in the literature, such as Hirsch (1988a). Therefore, they are not repeated here.

One way to discretize Eq. (1) is to adopt the FV framework. Thus, Eq. (1) is integrated over an arbitrary Eulerian domain of constant volume $\mathbb{V}$, and outer surface S, as follows:

$$\int_{\mathbb{V}} \left(\frac{\partial \vec{Q}}{\partial t} \right) d\mathbb{V} + \int_{\mathbb{V}} \left(\nabla \cdot \vec{\mathcal{F}} \right) d\mathbb{V} = 0 \qquad \Longrightarrow \qquad \frac{\partial}{\partial t} \int_{\mathbb{V}} \vec{Q}\, d\mathbb{V} + \oint_S \vec{\mathcal{F}} \cdot \overrightarrow{dS} = 0 \,. \tag{5}$$

In Eq. (5), the Green-Gauss theorem has been applied in conjunction with the general form of the Leibniz rule. Moreover, $\overrightarrow{dS} \equiv \hat{n}\, dS$, where $\hat{n}$ is the unitary normal vector that points in the outward direction of S.

The computational domain is assumed to be divided into multiple discrete cells of polyhedral shape, composing an unstructured grid. The discrete conserved variables vector, $\vec{Q}_i$, associated with the i-th cell of finite volume $\mathbb{V}_i$, is defined as

$$\vec{Q}_i \equiv \frac{1}{\mathbb{V}_i} \int_{\mathbb{V}_i} \vec{Q}\, d\mathbb{V} \,. \tag{6}$$

If n_f is the number of faces of a cell, then Eq. (5) becomes

$$\mathbb{V}_i \frac{\partial \vec{Q}_i}{\partial t} + \sum_{k=1}^{n_f} \left(\vec{\mathcal{F}}_k \cdot \vec{S}_k \right) = 0 \qquad \Longrightarrow \qquad \frac{\partial \vec{Q}_i}{\partial t} = -\frac{1}{\mathbb{V}_i} \sum_{k=1}^{n_f} \left(\vec{\mathcal{F}}_k \cdot \vec{S}_k \right) , \tag{7}$$

after applying a 1-point Gaussian quadrature rule, which is sufficient for a second-order scheme.

Equation (7) is the finite volume discretization of the RANS equations and is applied to all cells in the domain. For a mesh of constant geometry, the face area vectors, $\vec{S}_k$, are known at all times. Consequently, only two procedures are yet to be established: the reconstruction scheme used for the evaluation of the face flux vectors, $\vec{\mathcal{F}}_k$, as well as a procedure for integrating $\partial \vec{Q}_i / \partial t$ over time. Here, Roe's second-order TVD scheme (Roe, 1981), coupled with Venkatakrishnan's limiter (Venkatakrishnan, 1995), is used in the discretization of all inviscid fluxes (Bigarella and Azevedo, 2009, 2012), including the ones related to the turbulence model. The integration of the temporal derivatives is performed by using an implicit time-march scheme, as described in Bigarella and Azevedo (2009, 2012). These schemes were chosen as part of an effort to improve the overall robustness of the solution process. Hence, the only remaining issue is to define a scheme for computing the viscous fluxes.

The calculation of the viscous components of $\overrightarrow{\mathcal{F}}_k$ requires the reconstruction of both $\vec{Q}$ and $\overrightarrow{\nabla Q}$ at the k-th cell face. In the present formulation, a centered approach is followed. Therefore, if i and j are the indexes of two adjacent cells, then:

$$\vec{Q}_k = \frac{\vec{Q}_{k_i} + \vec{Q}_{k_j}}{2} , \tag{8}$$

in which $\vec{Q}_{k_i}$ and $\vec{Q}_{k_j}$ are the piecewise reconstructed properties of i and j, respectively, evaluated at the centroid of the k-th face (Barth and Jespersen, 1989). Based on the same idea, $(\overrightarrow{\nabla Q})_k$ is also reconstructed as a function of the directly adjacent cell discrete properties. The definition of this function is what sets the gradient reconstruction procedures apart from each other. In the next subsection, the three gradient reconstruction procedures considered here are briefly presented.

2.2 Gradient Reconstruction Schemes

2.2.1 Weighted Green-Gauss Gradient Scheme

The evaluation of a property gradient at a cell interface usually involves the definition of a reconstruction procedure that utilizes known information from the directly adjacent cells. The selection of a suitable reconstruction depends on multiple factors, such as the problem configuration and the available computational resources. In the present work, three different gradient reconstruction procedures are considered: $A00$, $A0E$ and $AJ0$, following the naming conventions from Jalali *et al.* (2014). Other reconstruction schemes do exist, as described, for instance, in Jalali *et al.* (2014) and Nishikawa (2010, 2011), but only these three are analyzed here due to their simplicity and overall computational efficiency.

All reconstruction schemes analyzed here are a function of the discrete cell property gradient. Therefore, it is necessary to define a method for computing it before presenting the formulation of each cell-interface gradient reconstruction scheme. Here, a Green-Gauss approach is adopted (Blazek, 2015). If A is defined as a property whose discrete values, A_i, are known at each cell, then its average cell gradient, $(\overrightarrow{\nabla A})_i$, after some algebraic manipulation can be computed as

$$(\overrightarrow{\nabla A})_i \equiv \frac{1}{\mathbb{V}_i} \int_{\mathbb{V}_i} \overrightarrow{\nabla A} \, d\mathbb{V} = \frac{1}{\mathbb{V}_i} \oint_S A \, d\vec{S} = \frac{1}{\mathbb{V}_i} \sum_{k=1}^{n_f} A_k \, \vec{S}_k \, . \tag{9}$$

Once gain, the interface properties, A_k, are computed by using some sort of average between the adjacent known values. A volume-weighted average is used here, as follows:

$$A_k = \frac{\mathbb{V}_i A_i + \mathbb{V}_j A_j}{\mathbb{V}_i + \mathbb{V}_j} \, . \tag{10}$$

More robust, but more computationally expensive, schemes for computing cell-averaged property gradients are also available in the literature, such as the Linear Preserving Gradient (LPG) and the Least Squares (LS) family of methods (Cary *et al.*, 2009).

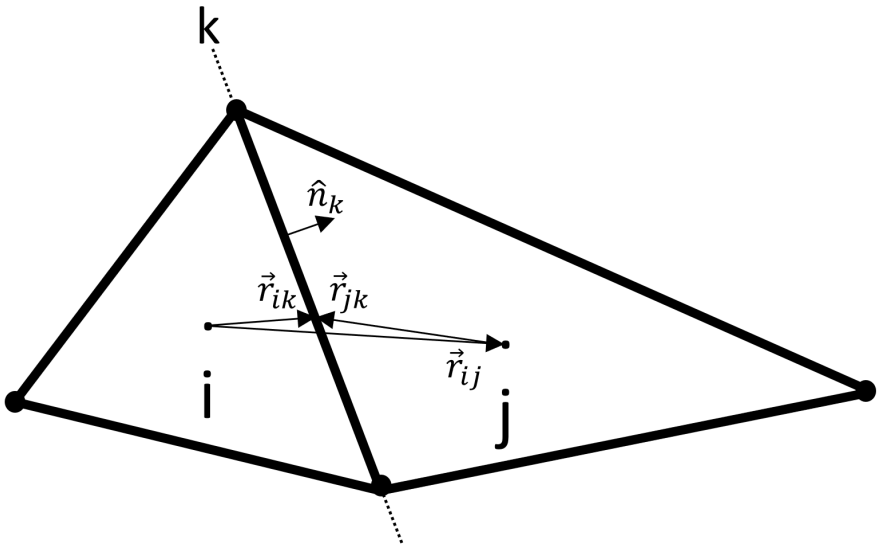

Figure 1. Mesh schematic diagram picturing cells i and j. Focus is given to the k-th face of the i-th cell. Face normal unitary vector, $\hat{n}_k$, as well as relevant distance vectors, $\vec{r}$, are also shown. The dots are used to represent the cell centroid locations.

2.2.2 Scheme A00

The first gradient reconstruction procedure presented here, $A00$, is perhaps the simplest formulation possible. It consists of a simple average between the two directly adjacent cell values:

$$(\overrightarrow{\nabla A})_k = \frac{(\overrightarrow{\nabla A})_i + (\overrightarrow{\nabla A})_j}{2} \equiv (\overline{\nabla A})_k \, . \tag{11}$$

This reconstruction can also be improved by, instead, using a weighted average (Jalali *et al.*, 2014), without loss of computational efficiency. However, only the formulation shown in Eq. (11) is considered in the present effort. In the same equation, a new term, $(\overline{\nabla A})_k$, has been defined in order to simplify the formulation of other equations throughout this document.

Although extremely cheap to compute, the usage of this scheme results in a stencil that effectively does not utilize information from the i and j cells (Blazek, 2015; Weiss *et al.*, 1998). In turn, high-frequency errors can develop in the solution (Jalali *et al.*, 2014). To solve this problem, the formulation from Eq. (11) is augmented by the introduction of extra terms that ensure dependency on cell-averaged data of the two cells that share the interface. Schemes $A0E$ and $AJ0$ are inserted in this category.

2.2.3 Scheme A0E

The $A0E$ scheme, also known as the edge-normal scheme, is one of the possible solutions for the previously mentioned $A00$ problem. It consists in exchanging the gradient component in the direction that connects the i and j cell centroids with a finite difference construct (Jalali *et al.*, 2014; Weiss *et al.*, 1998). Following the diagram illustrated in Fig. 1, the $A0E$ formulation can be written as

$$(\overrightarrow{\nabla A})_k = (\overline{\nabla A})_k + \left[\frac{A_j - A_i}{|\vec{r}_{ij}|} - (\overline{\nabla A})_k \cdot \frac{\vec{r}_{ij}}{|\vec{r}_{ij}|} \right] \frac{\vec{r}_{ij}}{|\vec{r}_{ij}|} \, . \tag{12}$$

Hence, cells i and j are effectively reintroduced to the stencil of $(\overrightarrow{\nabla A})_k$.

2.2.4 Scheme AJ0

Another approach is to use a jump term construct, $AJ0$, in which information from the discontinuous solution at the face center is introduced to the face gradient reconstruction (Jalali *et al.*, 2014; Nishikawa, 2010). The equation, then, becomes

$$(\overrightarrow{\nabla A})_k = (\overline{\nabla A})_k + \frac{\alpha}{|\vec{r}_{ij} \cdot \hat{n}_k|} \left(A_{k_j} - A_{k_i}\right) \hat{n}_k \,, \tag{13}$$

where A_{k_i} and A_{k_j} are the piecewise linear reconstructed A properties of cells i and j, respectively, evaluated at the face centroid. Furthermore, $\hat{n}_k$ is the face normal unitary vector pointing outwards from the current cell. For the $A0E$ scheme, the jump coefficient, α, is taken to be $\alpha = 4/3$.

It can be shown that multiple gradient reconstruction techniques can be cast into the form of Eq. (13) (Nishikawa, 2010). In fact, the $A0E$ scheme can be written by using Eq. (13) with the following α:

$$\alpha = (\hat{n}_k \cdot \hat{e}_{ij}) \, |\hat{n}_k \cdot \hat{e}_{ij}| \,, \tag{14}$$

where

$$\hat{e}_{ij} \equiv \frac{\vec{r}_{ij}}{|\vec{r}_{ij}|} \,. \tag{15}$$

The above expression for the $A0E$ scheme is the one that is effectively implemented here.

3. DESCRIPTION OF TEST CASES

3.1 Zero-Pressure Gradient Flat Plate

The flat plate case follows NASA Langley's Turbulence Modeling Resource (TMR) setup (Rumsey, 2022). Hence, it is an essentially incompressible case solved by using a compressible fluid formulation. The problem consists of a simple rectangular domain with a length of 2.33 m and a height of 1 m. The first 0.33 m of the bottom boundary is a symmetry plane. An infinitely thin flat plate, which is modeled as an adiabatic no-slip wall, lies in the other 2 m. A diagram that illustrates the problem can be seen in Fig. 2. The same figure also shows the enforced boundary conditions. Freestream properties are computed based on the known freestream Mach number, M_∞, reference temperature, T_∞, and Reynolds number, Re_∞, based on the reference length, ℓ_{ref}, as shown in Tab. 1.

Table 1. Freestream conditions for the zero-pressure gradient flat plate case.

Re_∞	M_∞	ℓ_{ref}	T_∞
5×10^6	0.2	1 m	300.00 K

Since BRU3D is a 3-D code, a quadrilateral mesh is simulated by using hexahedral meshes with a single cell depth-wise. The mesh employed here is the finest hexahedral mesh available in the TMR website (Rumsey, 2022), and is composed of 544 cells in the X direction and 384 cells in the Y direction. Cells are clustered in the region near the leading edge of the flat plate, as seen in Fig. 3.

3.2 OAT15A Airfoil

The second case is the transonic OAT15A airfoil, described in Roddle and Archambaud (1994). The domain has two boundary conditions: no-slip adiabatic wall, enforced over the airfoil surface, and non-reflective farfield, imposed over the outer surface of the domain. The freestream conditions are presented in Tab. 2, where c is the airfoil chord length and α_{AoA} is the flow angle of attack. The mesh is constructed with 410 cells distributed along the airfoil chord. The farfield is located at 240 chords away from the airfoil surface. Cells are clustered around the airfoil surface, in such a way that $y^+ \approx 1$ at the no-slip wall, as depicted in Fig. 4.

Table 2. Freestream conditions for the transonic OAT15A airfoil case.

Re_∞	M_∞	c	T_∞	α_{AoA}
3×10^6	0.724	1 m	246.66 K	1.15 deg.

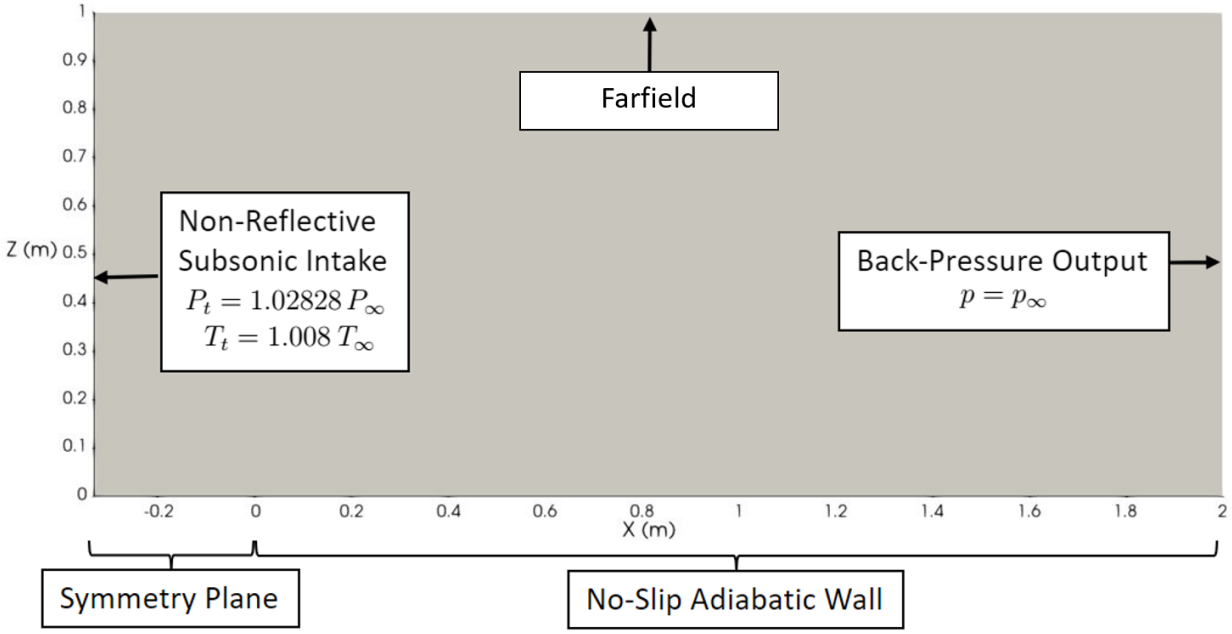

Figure 2. Boundary condition placement for the two-dimensional, zero-pressure gradient, flat plate case.

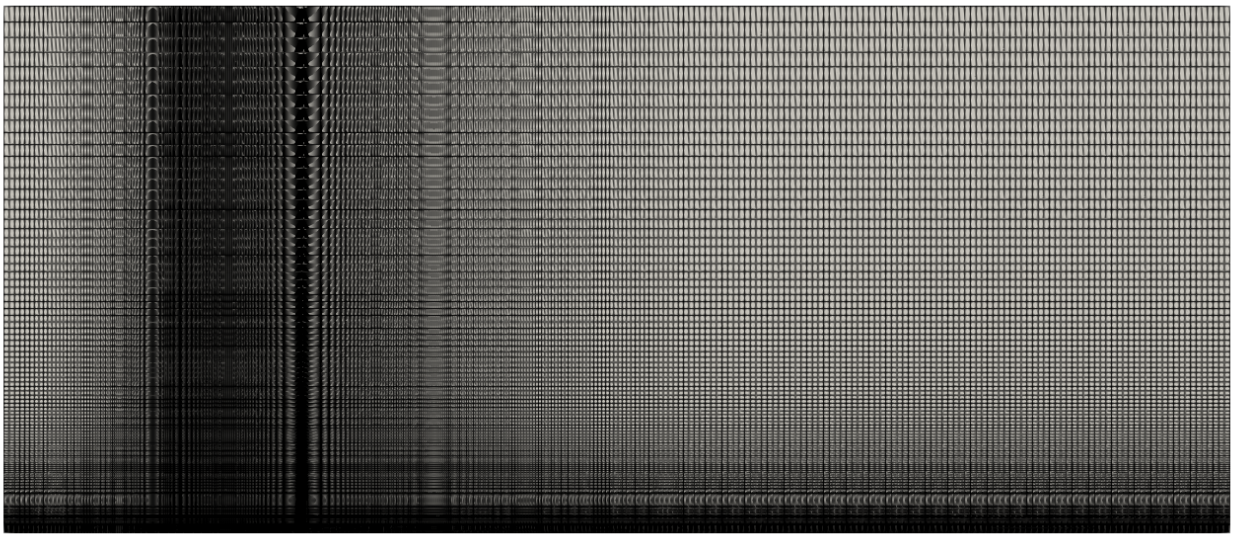

Figure 3. Mesh used in the flat plate case, containing 544 x 384 cells.

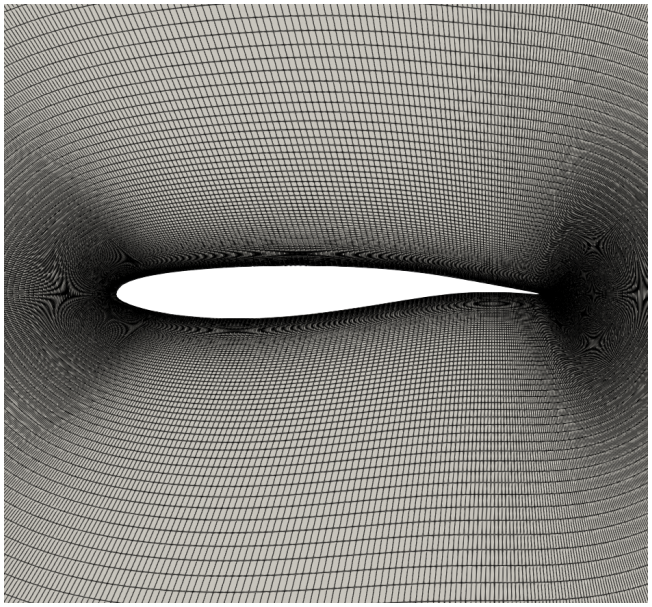

Figure 4. Zommed-in view of the mesh used in the transonic OAT15A airfoil case.

4. RESULTS AND DISCUSSION

4.1 Zero-Pressure Gradient Flat Plate

Values of skin-friction coefficient, c_f, plotted along the length of the flat plate are shown in Fig. 5. The skin friction coefficient is defined as

$$c_f \equiv \frac{\tau_w}{\frac{1}{2}\rho_\infty u_\infty^2} \,, \tag{16}$$

in which τ_w is the fluid shear stress measured at the wall. Experimental data from Coles and Hirst (1969), along with von Kármán's empirical curve (White, 2006) are also shown for comparison. The von Kármán empirical curve is defined as

$$C_{f_{vonKrmn}} \approx \frac{0.027}{(Re_x)^{\frac{1}{7}}} \,. \tag{17}$$

Simulation data from TMR (Rumsey, 2022), obtained using NASA's CFL3D and FUN3D codes using the Spalart-Allmaras turbulence model, are also plotted. It is clear that, despite slight changes being visible between the experimental data and most of the simulation data, the results obtained by the three different gradient reconstruction schemes are virtually identical in the context of the current case setup. This observation is also valid when comparing the current data to the simulation results obtained by using CFL3D and FUN3D. Figure 6 shows a zommed-in view of Fig. 5. It highlights the fact that the numerically computed c_f values differ from each other by a maximum of, approximately, 0.1%. This difference is, for engineering purposes, negligible, which shows that the numerical results from Fig. 5 are not dependent on the discretization techniques being currently considered. Therefore, differences between experimental data and simulation data can be attributed to the turbulence model adopted and not to the gradient reconstruction technique in use.

4.2 Transonic OAT15A Airfoil

The OAT15A airfoil is a transonic case and, therefore, shock waves are expected to develop in the discrete solution. Distribution of c_p along the chord of the OAT15A airfoil is shown in Fig. 7, compared against experimental data from Roddle and Archambaud (1994). Likewise, no meaningful differences are observed in the obtained results, using the three different schemes, throughout the entire length of the airfoil. This is true even in regions close to the shock wave, as seen from Fig. 8, where an extremely zoomed-in view is presented in order to visualize separate curves.

Computed aerodynamic coefficients, in the form of c_L and c_D, are shown in Tab. 3. Interpolated data are extracted from the plots available in Roddle and Archambaud (1994). There is a significant disparity between the computed coefficients and the experimental values. This is, however, a known limitation of the Spalart-Allmaras turbulence model, due to its inability to correctly solve the shock wave location for this case, as shown by Bigarella and Azevedo (2009, 2012).

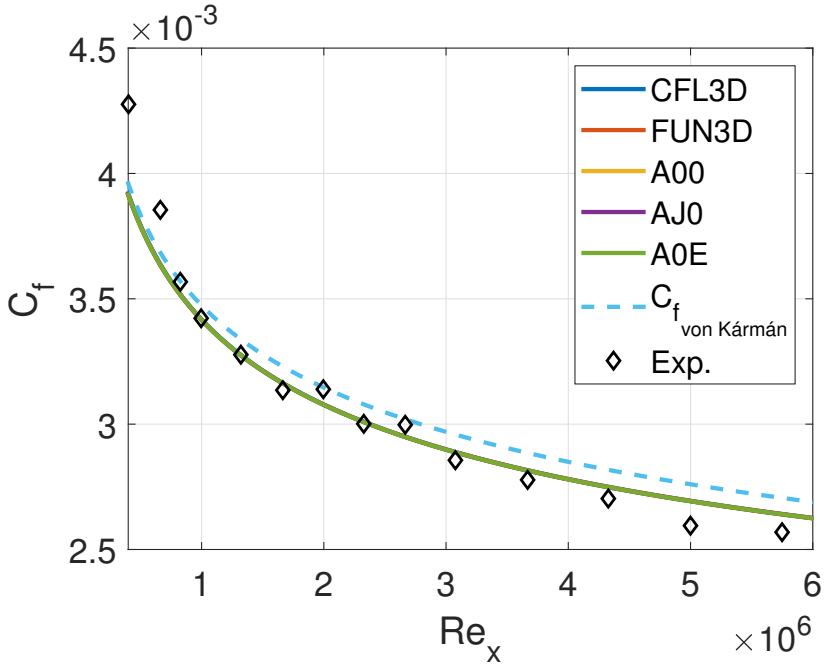

Figure 5. Skin friction coefficient distribution, c_f, as a function of Re_x, along the first 1.2 m of the flat plate. Experimental data from Coles and Hirst (1969) are added for comparison.

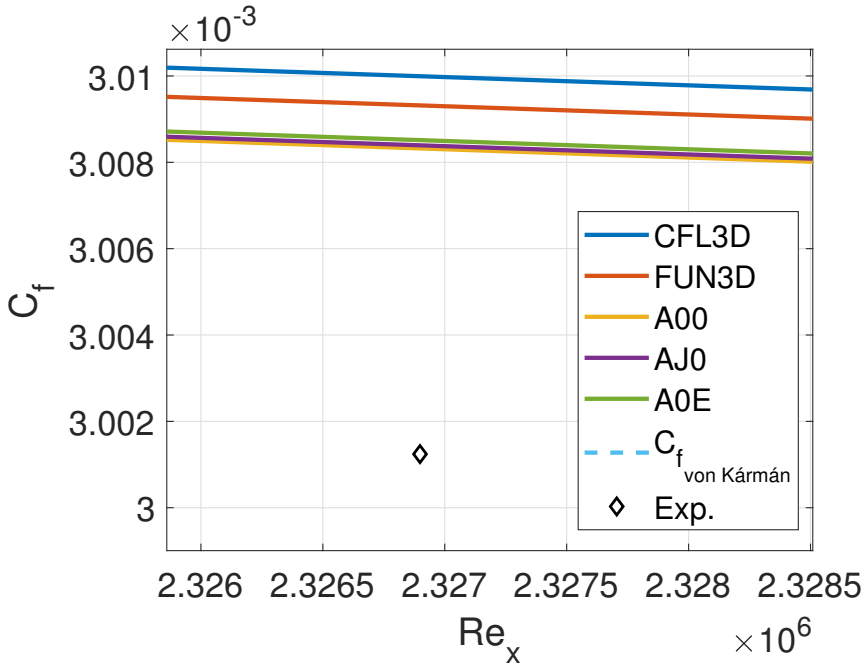

Figure 6. Zoomed-in view of Fig. 5, which highlights the small differences between all numerical results.

Table 3. Comparison between computed aerodynamic coefficients and interpolated experimental data for the transonic OAT15A airfoil case.

Source	c_L	c_D
BRU3D V00	0.69178	0.013152
BRU3D AJ0	0.69163	0.013197
BRU3D A0E	0.69183	0.013183
Interp. Exp. Data	0.5949	0.0106

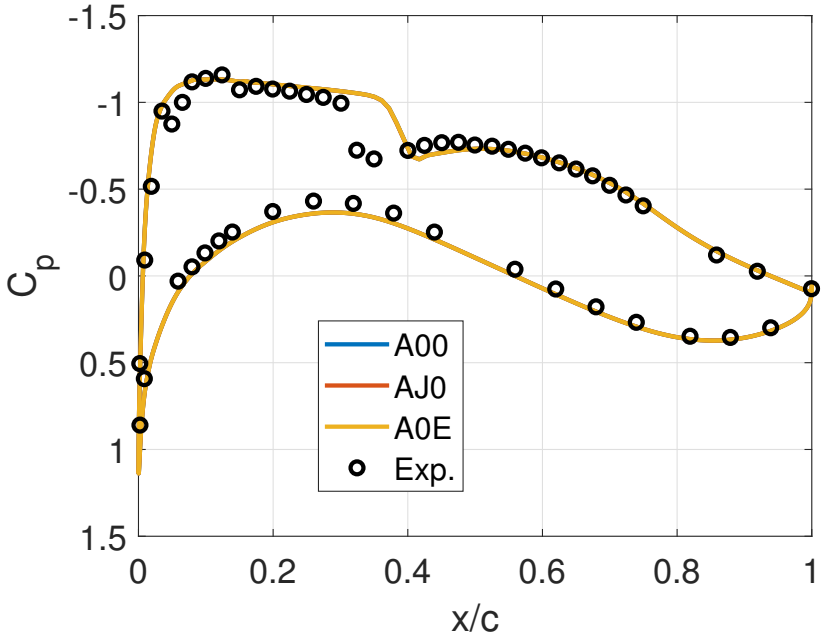

Figure 7. Pressure coefficient, c_p, distribution along the airfoil surface for the transonic OAT15A case.

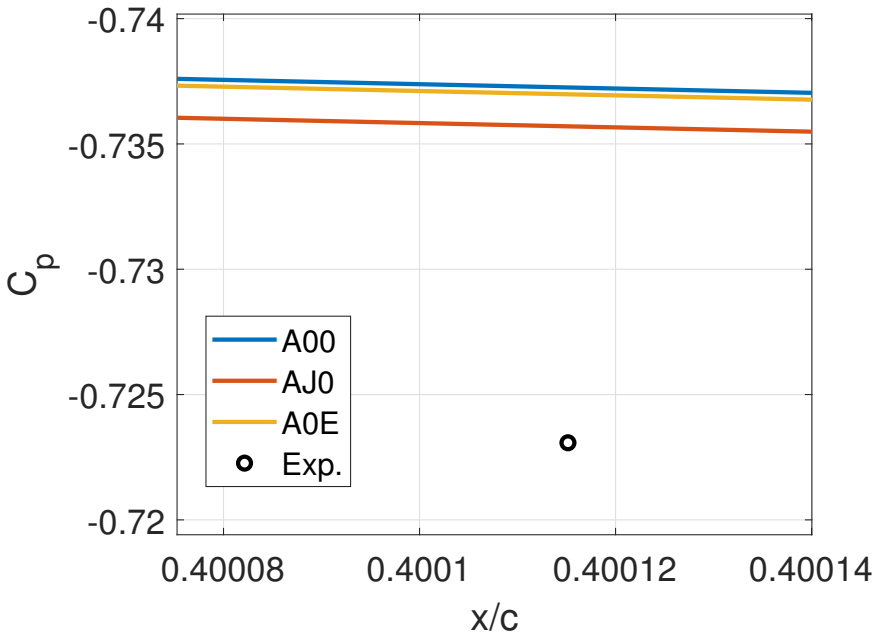

Figure 8. Zoomed-in view of Fig. 7 in the region near the airfoil upper surface shock wave.

5. CONCLUDING REMARKS

The current research effort analyzed the performance of three different gradient reconstruction techniques when solving two different two-dimensional, steady-state, turbulent cases. Special attention is given to problems formulated using quadrilateral meshes. No meaningful difference is observed between the results obtained using the different reconstruction schemes, at least in regards to the test cases taken into account. Therefore, for problems of similar configuration to the ones shown here, CFD users can theoretically utilize any gradient reconstruction technique they prefer, with virtually no loss of accuracy. The authors, however, emphasize that this recommendation is limited to the use of quadrilateral meshes on problems which are essentially two-dimensional, where high-orthogonality cells are usually present. In the context of a more general mesh, especially for truly three-dimensional problems, where ill-conditioned cells might be present, this conclusion may no longer be valid. Hence, more pronounced differences are expected to be seen in the results produced by each gradient reconstruction scheme for these more complex cases. This issue is precisely what the authors are addressing as a continuation of the present effort.

6. ACKNOWLEDGEMENTS

The authors wish to express their gratitude to the São Paulo Research Foundation, FAPESP, which has supported the present research under the Research Grants No. 2021/00147-8 and No. 2013/07375-0. The authors also gratefully acknowledge the support for the present research provided by Conselho Nacional de Desenvolvimento Científico e Tecnológico, CNPq, under the Research Grant No. 309985/2013-7. The work is further supported by the computational resources of the Center for Mathematical Sciences Applied to Industry (CeMEAI), also funded by FAPESP under the Research Grant No. 2013/07375-0.

7. REFERENCES

Allmaras, S.R., Johnson, F.T. and Spalart, P.R., 2012. "Modifications and Clarifications for the Implementation of the Spalart-Allmaras Turbulence Model". AIAA Paper No. 2007-4079, *7th International Conference on Computational Fluid Dynamics (ICCFD7)*, Big Island, Hawaii, USA.

Barth, T.J. and Jespersen, D.C., 1989. "The Design and Application of Upwind Schemes on Unstructured Meshes". AIAA Paper No. AIAA-89-0366, *27th AIAA Aerospace Sciences Meeting*, Reno, Nevada, USA.

Bigarella, E.D.V. and Azevedo, J.L.F., 2009. "A Unified Implicit CFD Approach for Turbulent-Flow Aerospace-Configuration Simulations". AIAA Paper No. 2009-1473, *47th AIAA Aerospace Sciences Meeting including The New Horizons Forum and Aerospace Exposition*, Orlando, Florida, USA.

Bigarella, E.D.V. and Azevedo, J.L.F., 2012. "A Study of Convective Flux Schemes for Aerospace Flows". *Journal of the Brazilian Society of Mechanical Sciences and Engineering*, Vol. 34, No. 3, pp. 314–329.

Blazek, J., 2015. *Computational Fluid Dynamics: Principles and Applications*. Butterworth-Heinemann, Elsevier, Oxford, UK, 3rd edition.

Cary, A., Dorgan, A. and Mani, M., 2009. "Towards Accurate Flow Predictions Using Unstructured Meshes". AIAA Paper No. 2009-3650, *19th AIAA Computational Fluid Dynamics*.

Coles, D. and Hirst, E.A., 1969. "Computation of Turbulent Boundary Layers". Proceedings of the 1968 U.S. Air Force Office of Scientific Research - Internal Flow Program - Stanford Conference, Stanford University Press, Palo Alto, CA, USA.

Hirsch, C., 1988a. *Numerical Computation of Internal and External Flows - Volume 1: Fundamentals of Numerical Discretization*, Wiley, Chichester, p. 515. 1st edition.

Hirsch, C., 1988b. *Numerical Computation of Internal and External Flows - Volume 2: Computational Methods for Inviscid and Viscous Flows*, Wiley, Chichester, p. 691. 1st edition.

Jalali, A., Sharbatdar, M. and Ollivier-Gooch, C., 2014. "Accuracy Analysis of Unstructured Finite Volume Discretization Schemes for Diffusive Fluxes". *Computers & Fluids*, Vol. 101, pp. 220–232.

Nishikawa, H., 2010. "Beyond Interface Gradient: A General Principle for Constructing Diffusion Schemes". AIAA Paper No. 2010-5093, *40th Fluid Dynamics Conference and Exhibit*.

Nishikawa, H., 2011. "Robust and Accurate Viscous Discretization via Upwind Scheme – I: Basic Principle". *Computers & Fluids*, Vol. 49, No. 1, pp. 62–86.

Roddle, A.M. and Archambaud, J.P., 1994. "OAT15A Airfoil Data". *A Selection of Experimental Test Cases for the Validation of CFD Codes*, AGARD-AR-303, NATO Advisory Group for Aerospace Research & Developtment, Case A11.

Roe, P.L., 1981. "Approximate Riemann Solvers, Parameter Vectors and Difference Schemes". *Journal of Computational Physics*, Vol. 43, No. 2, pp. 357–372.

Rumsey, C., 2022. "NASA's Langley Research Center - Turbulence Modeling Resource Website". Available in `https://turbmodels.larc.nasa.gov/`. Last accessed in 08 Jun. 2022.

Spalart, P.R. and Allmaras, S.R., 1992. "A One-Equation Turbulence Model for Aerodynamic Flows". AIAA Paper No. 92-0439, *30th Aerospace Sciences Meeting & Exhibit*, Reno, NV, USA.

Venkatakrishnan, V., 1995. "Convergence to Steady State Solutions of the Euler Equations on Unstructured Grids with Limiters". *Journal of Computational Physics*, Vol. 118, pp. 120–130.

Weiss, J.M., Maruszewski, J.P. and Smith, W.A., 1998. "Implicit Solution of Preconditioned Navier-Stokes Equations Using Algebraic Multigrid". *AIAA Journal*, Vol. 37, No. 1, pp. 29–36.

White, F.M., 2006. *Viscous Fluid Flow*, McGraw Hill, New York, USA, p. 629. 3rd edition.

8. RESPONSIBILITY NOTICE

The authors are solely responsible for the printed material included in this paper.